

D-STATCOM for harmonic mitigation in low voltage distribution network with high penetration of nonlinear loads

Wesam Rohouma^{a, *}, Robert S. Balog^a, Aaqib Ahmad Peerzada^b, Miroslav M. Begovic^b

^a *Renewable Energy & Advanced Power Electronics Research Laboratory, Department of Electrical & Computer Engineering, Texas A&M University at Qatar, Doha, Qatar*

^b *Department of Electrical & Computer Engineering, Texas A&M University, College Station, TX, USA*

ARTICLE INFO

Article history:

Received 6 December 2018

Received in revised form

5 May 2019

Accepted 31 May 2019

Available online 1 June 2019

Keywords:

D-STATCOM

Power quality

Reactive power compensation

Harmonic compensation

Matrix converter

Power factor correction

ABSTRACT

With the increased use of power electronic for ac-to-dc converters, electrical distributions systems are experiencing an increased in non-linear loads. These non-linear loads, such as the classical rectifier, draw non-sinusoidal currents which tend to have a deleterious impact on the power quality of the modern AC distribution systems. The interaction of non-sinusoidal currents with the grid impedance leads to distorted system voltage which can adversely impact other devices connected to the grid. The integration of distributed energy resources (DERs) with the distribution power grid can further exacerbate the harmonic power issues. The traditional methods of compensation are no longer adequate and hence it is necessary to develop a means to provide local reactive and harmonic compensation at the source of the power quality problem within the low-voltage distribution network. This article investigates the use of a capacitor-less distribution static synchronous compensator (D-STATCOM) for power quality compensation in modern distribution systems. The proposed topology is based on a matrix converter (MC), controlled by finite control set model predictive control (FCS-MPC) which makes possible the use of inductive energy storage rather than electrolytic capacitors, which have been proven to be the most failure-prone components in a power electronic circuit. Simulation and experimental results are presented to validate the effectiveness of the approach.

© 2019 The Authors. Published by Elsevier Ltd. This is an open access article under the CC BY-NC-ND license (<http://creativecommons.org/licenses/by-nc-nd/4.0/>).

1. Introduction

The National Academy of Engineers (NAE) identified the electricity grid (electrification) as one of the greatest achievements of the 20th century [1]. Invented by Tesla and implemented by Westinghouse, the electrical power grid spurred the second industrial revolution in which factories were driven by electrical motors and the night was light up by incandescent lamp. A century later, the characteristic of the loads has changes and society's appetite for electrical energy only continues to grow with consumers demanding both increased quantity and quality of electrical power [2]. Continuous power supply and improved power quality are critical for the post-industrial, digital economy which is increasingly based on the continuous real-time flow of information.

For many e-commerce and digital economy based businesses, power outages are unacceptably expensive [3–5]. The Department of Energy (DOE) estimates the cost of power outages per hour for a brokerage business to be \$6.5 million, while credit card business costs around \$2.5 million [6,7]. In Europe, it is estimated that power quality problems cost industry and commerce about 10 billion euro per annum; the cost to address this problem is estimated to be only 5% of the this cost [8,9].

The use of power electronics based loads such as variable speed drives, inverter-based air-conditioning, distributed generation and storage systems, solid-state LED lights, personal electronics, and electric vehicles, has given rise to problems related to power quality in distribution network [10–12], as illustrated in Fig. 1. The problems and challenges related to the integration of the power electronics enabled loads can be grouped into PQ issues such as current and voltage harmonics, voltage rise, voltage unbalance and instability. Operational issues including malfunctioning of protection equipment, overloading of cables and transformers, and increased system losses [13–16].

Traditionally, power-quality issues have been addressed by the

* Corresponding author.

E-mail addresses: wesam.rohouma@qatar.tamu.edu (W. Rohouma), robert.balog@ieee.org (R.S. Balog), peerzada@tamu.edu (A.A. Peerzada), begovic@tamu.edu (M.M. Begovic).

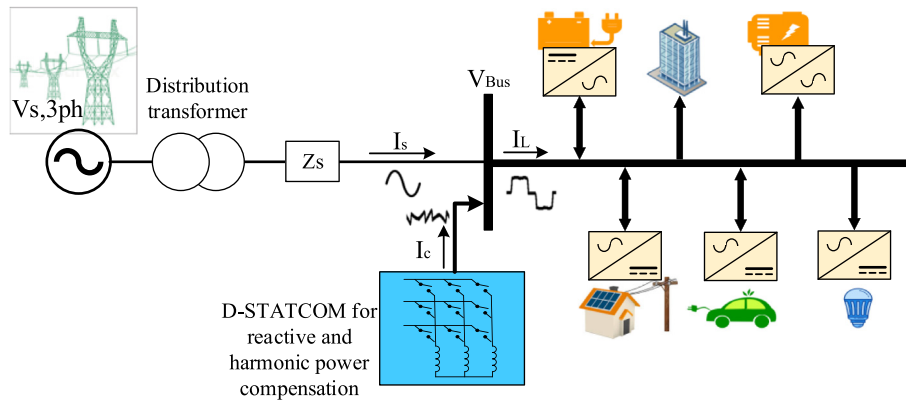


Fig. 1. One-line diagram of a distribution network.

use basic devices such as passive filters, and more advanced filtering technologies, such as a static synchronous compensator, active power filter (APF), dynamic voltage regulator, and unified power quality conditioner (UPQC) [17–20]. Passive filters have been traditionally used to improve the power quality of the electrical network. However, they have several issues such as resonance, fixed filter frequency, and difficulty in tuning [21–23]. Researchers have proposed the active power filter (APF) which is developed to remedy the shortcomings of the passive filter has made it possible to mitigate various power quality problems such as harmonic and reactive power compensation, voltage imbalance, voltage flicker. Researchers also have proposed that PV inverters embedded with smart inverter control algorithms can be used to improve the power quality by providing harmonic current compensation. However, this reduces inverter reliability and adds additional complexity and cost [10,24–26]. On the other hand, the backbone of both APF and PV inverters is the voltage source inverter (VSI), with electrolytic capacitors. These capacitors are subjected to accelerated failures, especially in hot/arid environments [27,28] and are attributed to 30% of the failures that occur in power electronics [29–31]. At the same time, the life expectancy of components in the distribution system is measured in decades, with 50% of the copper & steel transformers in the power distribution system have been in service for 30 years and longer [2].

In this paper, the use of a capacitor-less distribution static synchronous compensator (D-STATCOM) for harmonic and reactive power compensation in a distribution network is investigated. The proposed topology is based on a matrix converter (MC) which is

controlled using finite control set model predictive control (FCS-MPC). This arrangement enables the use of inductive energy storage instead of electrolytic capacitors so that the compensator can meet the expectations of long service life as the existing distribution transformers. The compensator can be deployed and dispatched within the distribution feeder system, as needed, to compensate locally at the source of the problem. Simulation using MATLAB/Simulink and experiment using a testbed of 7.5kVA has been used to investigate the performance and capability of the proposed technology to mitigate power quality (PQ) issues in the distribution network.

2. System configuration

The D-STATCOM is a power electronic based reactive power compensation device that is shunt-connected at a particular bus in the electrical distribution system. The main building block in the proposed capacitor-less configuration is the three-phase matrix converter. Nine bi-directional switches, three-phase input filter and output chokes connected to the output side of the converter. Fig. 1 shows a simplified diagram of the proposed capacitor-less D-STATCOM configuration connected at the terminal bus in the distribution network. Upstream, toward the substation, is modelled as three-phase source with series impedance (Z_s). Downstream is modelled as two blocks, the first block is the harmonics generator block, this block is prosumer (producer-consumer) and it will generate harmonic currents to represent the aggregate behaviour of photovoltaic system with three-phase inverter and other

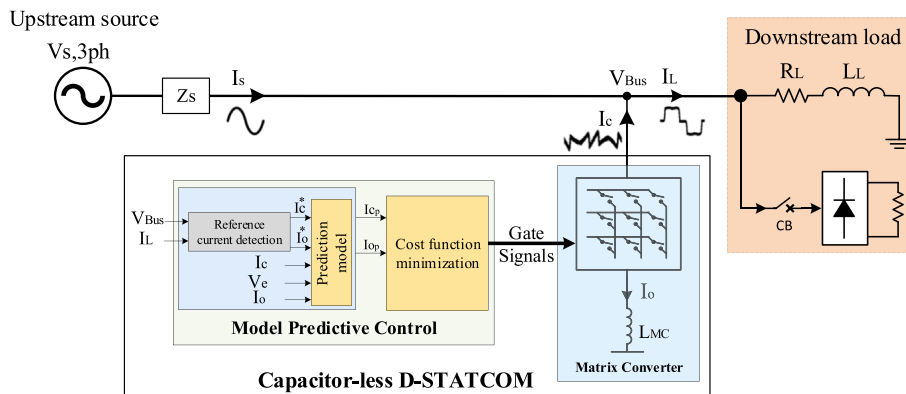


Fig. 2. Capacitor-less D-STATCOM based matrix converter.

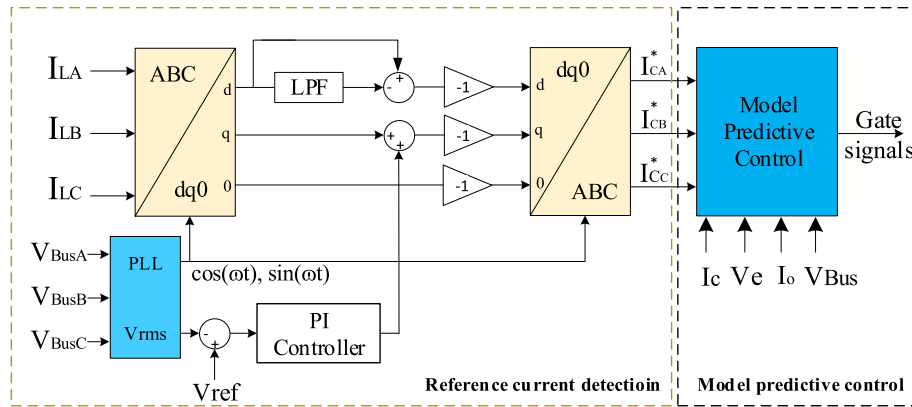


Fig. 3. Reference current detection based on synchronous reference frame (SRF).

harmonics producing loads such as personal computers, television sets, energy efficient lamps (fluorescent and LED). Similarly, the second load is the linear loads that are lumped into equivalent R-L load as shown in Fig. 2. The proposed D-STATCOM is shunt-connected and injects current (I_c) to compensate for the downstream operation such that current drawn from the upstream source (I_s) is sinusoidal and in phase with the voltage. Fig. 2 shows additional details of the system and the proposed capacitor-less D-STATCOM. The D-STATCOM in the figure consists of MC unit connected to the output chokes and controller unit consists of the reference current generator and the MPC.

3. Control of the power converter

The performance of the converters depends primarily on the control strategy and the reference current detection technique used. FCS-MPC is used to control the converter and the weight factors are manually tuned in this paper. Regarding the reference current detection, synchronous rotating reference frame (SRF) method has been adopted in this paper [32,33].

3.1. Reference current detection using SRF

To detect the load current harmonics, the load currents and voltages are measured, filtered, and reference currents are extracted according to the synchronous reference frame (SRF) method. SRF theory is based on the transformation of currents in synchronously rotating $d-q$ frame [26,34,35]. The transformation to the $d-q$ reference frame from the ABC reference frame is given in (1):

$$\begin{bmatrix} I_d \\ I_q \\ I_0 \end{bmatrix} = \frac{\sqrt{2}}{3} \begin{bmatrix} \cos(\omega t) & \cos(\omega t - 2\pi/3) & (\omega t + 2\pi/3) \\ -\sin(\omega t) & -\sin(\omega t - 2\pi/3) & -\sin(\omega t + 2\pi/3) \\ 1/\sqrt{2} & 1/\sqrt{2} & 1/\sqrt{2} \end{bmatrix} \cdot \begin{bmatrix} I_{LA} \\ I_{LB} \\ I_{LC} \end{bmatrix} \quad (1)$$

The block diagram of the SRF method is shown in Fig. 3. The three-phase load current is measured then transformed to the $dq0$ reference frame to extract the active and reactive current components of the load current; the new components consist of DC part that represents the fundamental component of the current and the AC part that represent the harmonics. Using a high pass filter (HPF), the harmonic component can be extracted and then transformed back to the ABC reference frame to be used as a reference current for the controller.

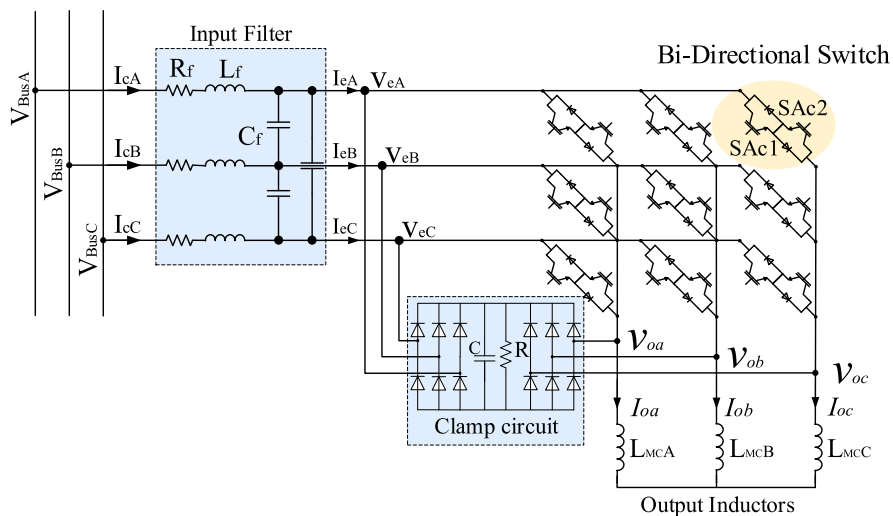


Fig. 4. Detailed D-STATCOM matrix converter based system.

3.2. Matrix converter model

The direct matrix converter (DMC) topology is used in this application. It consists of nine bidirectional switches each comprised of two IGBT and diode pairs connected in anti-parallel to support bidirectional current flow as shown in Fig. 4 which shows the detailed capacitor-less D-STATCOM system. The MC is connected to the bus through an input filter L_f , C_f , R_f , which is used to eliminate switching-frequencies and harmonics from propagating to the rest of the network. The output voltages and input currents of the MC were calculated according to (2) and (3) as a function of MC input voltages, output currents and the switching function. The inductive load constrains the switching to avoid interruption of MC output current. Where the voltage-source input constrains the switching to avoid shorting the input phases given in (4).

$$\begin{bmatrix} v_{oa} \\ v_{ob} \\ v_{oc} \end{bmatrix} = \begin{bmatrix} S_{Aa} & S_{Ba} & S_{Ca} \\ S_{Ab} & S_{Bb} & S_{Cb} \\ S_{Ac} & S_{Bc} & S_{Cc} \end{bmatrix} \cdot \begin{bmatrix} V_{SA} \\ V_{SB} \\ V_{SC} \end{bmatrix} \quad (2)$$

$$\begin{bmatrix} I_{inA} \\ I_{inB} \\ I_{inC} \end{bmatrix} = \begin{bmatrix} S_{Aa} & S_{Ab} & S_{Ac} \\ S_{Ba} & S_{Bb} & S_{Bc} \\ S_{Ca} & S_{Cb} & S_{Cc} \end{bmatrix} \cdot \begin{bmatrix} I_{oa} \\ I_{ob} \\ I_{oc} \end{bmatrix} \quad (3)$$

$$S_{Aj} + S_{Bj} + S_{Cj} = 1 \quad (4)$$

where $V_{oa}(t)$, $V_{ob}(t)$ and $V_{oc}(t)$, $I_{oa}(t)$, $I_{ob}(t)$ and $I_{oc}(t)$ are the output voltages and currents of the matrix converter respectively. While, $V_{BusA}(t)$, $V_{BusB}(t)$ and $V_{BusC}(t)$, $I_{cA}(t)$, $I_{cB}(t)$ and $I_{cC}(t)$ are the input voltages and currents of the matrix converter, and $S_{ij}(t)$ is the switching function between the MC input phase with $i \in \{A,B,C\}$, and the MC output phase with $j \in \{a,b,c\}$. Proper choice of S will lead to a phase-reversal of the current so that the inductive load appears capacitive at the input to the MC to supply reactive power to the network [36,37].

3.3. Load model

The output currents, of the MC shown in Fig. 4, are modelled using the per-phase differential equation:

$$L_{MCj} \frac{di_{oj}(t)}{dt} = v_{oj}(t) - R_{L_{MCj}} i_{oj}(t) \quad (5)$$

where v_{oj} is the per-phase output voltage of the MC, i_{oj} is the per phase output current of the MC, L_{MCj} and $R_{L_{MCj}}$ is the per-phase inductance and parasitic resistance of the output chokes. To make the model compatible with the MPC formulation, the continuous time derivative in (5) is approximated using the forward Euler method for each k th discrete sample time steps:

$$\frac{di_{oj}(t)}{dt} \approx \frac{i_{oj}(k+1) - i_{oj}(k)}{T_s} \quad (6)$$

From (5) and (6), the discrete-time model estimates the current at the next sample ($k+1$) is given as

$$i_{oj}^p(k+1) = \left(1 - \frac{R_{L_{MCj}} T_s}{L_{MCj}}\right) i_{oj}(k) + \frac{T_s}{L_{MCj}} v_{oj}(k) \quad (7)$$

3.4. Input filter model

Input filters are required in power electronics converters to eliminate the high-order harmonics generated by converter switching to going back to the supply. The input filter shown in Fig. 4 can be represented using Kirchoff's voltage and current equations as:

$$V_{Busi}(t) = R_{fi} i_{ci}(t) + L_{fi} \frac{d}{dt} i_{ci}(t) + V_{ei}(t) \quad (8)$$

$$i_{ci}(t) = i_{ei}(t) + C_{fi} \frac{d}{dt} V_{ei}(t) \quad (9)$$

where V_{Busi} , V_{ei} are the per-phase input and output voltages of the filter and i_{ci} and i_{ei} are the input and output currents of the filter, R_{fi} is the per-phase parasitic resistance of the input inductors. The state space model of the filter can be written as:

$$\begin{bmatrix} V_{ei}^*(t) \\ i_{ci}^*(t) \end{bmatrix} = A_c \begin{bmatrix} V_{ei}(t) \\ i_{ci}(t) \end{bmatrix} + B_c \begin{bmatrix} V_{Busi}(t) \\ i_{ei}(t) \end{bmatrix} \quad (10)$$

$$\begin{bmatrix} V_{ei}^*(t) \\ i_{ci}^*(t) \end{bmatrix} = \underbrace{\begin{bmatrix} 0 & \frac{1}{C_f} \\ \frac{1}{L_f} & \frac{R_f}{L_f} \end{bmatrix}}_{A_c} \begin{bmatrix} V_{ei}(t) \\ i_{ci}(t) \end{bmatrix} + \underbrace{\begin{bmatrix} 0 & -\frac{1}{C_f} \\ \frac{1}{L_f} & 0 \end{bmatrix}}_{B_c} \begin{bmatrix} V_{Busi}(t) \\ i_{ei}(t) \end{bmatrix} \quad (11)$$

Finally, the discrete model of the input filter using zero-order hold and sample time T_s is given by:

$$\begin{bmatrix} V_{ei}(k+1) \\ i_{ci}(k+1) \end{bmatrix} = A_q \begin{bmatrix} V_{ei}(k) \\ i_{ci}(k) \end{bmatrix} + B_q \begin{bmatrix} V_{Busi}(k) \\ i_{ei}(k) \end{bmatrix} \quad (12)$$

$$A_q = e^{A_c T_s} \text{ and } B_q = \int_0^{T_s} e^{A_c(T_s-\tau)} B_c d\tau \quad (13)$$

3.5. MPC for D-STATCOM application

Fig. 2 illustrates the system structure with the proposed controller. The objectives here is to control input current of the converter so it will track the reference current, the reactive input power and output currents of the MC [37]. The input reactive power and the input current of the converter can be written in orthogonal coordinates as:

$$Q^p(k+1) = V_{Bus\beta}(k) i_{c\alpha}(k) - V_{Bus\alpha}(k) i_{c\beta}(k) \quad (14)$$

$$i_{cn}^p(k+1) = A_{q(2,1)} V_{en}(k) + A_{q(2,2)} i_{cn}(k) + B_{q(2,1)} V_{Busn}(k) + B_{q(2,2)} i_e(k) \quad (15)$$

where α and β are the real and imaginary components of the associated voltage and current vectors. $i_{cn}^p(k+1)$ is the predicted value of the D-STATCOM input current for the sampling interval ($k+1$).

The cost function J is given as

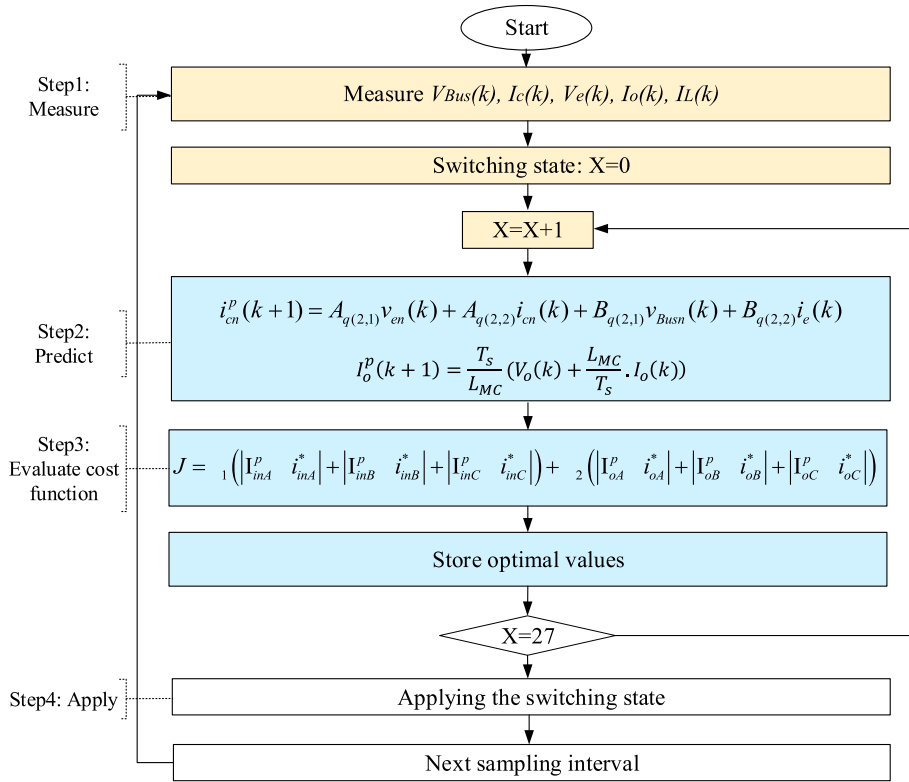


Fig. 5. Flow chart of the model predictive controller.

$$J = \lambda_1 (|I_{inA}^p - i_{inA}^*| + |I_{inB}^p - i_{inB}^*| + |I_{inC}^p - i_{inC}^*|) + \lambda_2 (|I_{oA}^p - i_{oA}^*| + |I_{oB}^p - i_{oB}^*| + |I_{oC}^p - i_{oC}^*|) \tag{16}$$

where J is the cost function and I_{CA} , I_{CB} and I_{CC} are the MC input currents, I_{oA} , I_{oB} and I_{oC} is the MC output currents. The weight factors λ_1 , λ_2 are adjusted to priorities the different parts of the cost function. Optimal tuning of these weight factor is still an open topic

for research [38,39]. In this paper, manual tuning of the weight factors is performed according to the guidelines from Ref. [39].

The MPC algorithm for the D-STATCOM control is shown in Fig. 5. In this flow chart, the first step is the measurement step where the measurements of the three-phase bus voltage, load current, matrix converter output choke current, matrix converter input voltages and currents are performed. The second step is a prediction. In this step, the controller will perform the prediction and cost function calculation for all the possible states. Weight factors λ_1 , and λ_2 are the controller parameters that need tuning, in this paper, these factors were manually tuned. In the manual

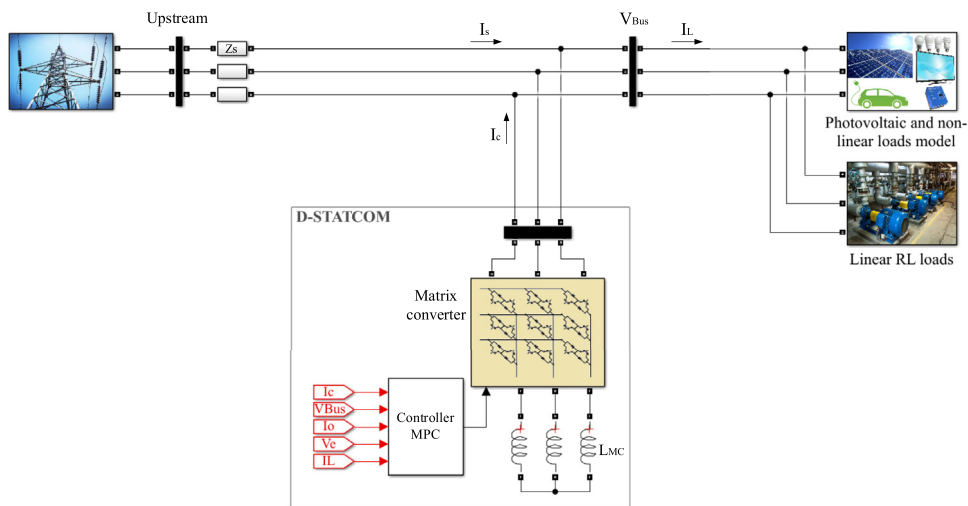


Fig. 6. Simulation model of the system.

Table 1
System parameters.

Parameter	Value
Voltage, $V_{LL,rms}$	415 V
Frequency	50 Hz
Source impedance (Z_s)	1 mH
Load resistance per phase R_L	30 Ω
Load inductance per phase L_L	120 mH
Output chokes inductance L_{MC}	36 mH
Input filter parasitic resistance R_f	2 Ω
Input filter inductance L_f	2 mH
Input filter capacitor $C_{f/ph}$	12 μ F
Three phase rectifier resistor R_{NLL}	125 Ω
Sampling time T_s	40 μ s
Weight factor λ_1	1
Weight factor λ_2	0.2

tuning, the value of λ_1 is kept at unity to provide good tracking of the D-STATCOM input current, and the value of λ_2 is changed from 0.05 to 1 with step of 0.02. And it has been found that the best value for λ_2 is 0.2 in this test. Step three is the optimization step in which the selection of the minimum cost function and the associated switching state is performed. In the last step, the selected switching state is applied to the converter switches.

4. Simulation and experimental results

The performance of the proposed capacitor-less D-STATCOM controlled by FCS-MPC has been verified in MATLAB/Simulink (R2017a) simulation environment. Simulation model have been built with the configuration shown in Figs. 2 and 4–6. Extensive simulations have been done for different use cases. The simulation results were validated further by an experimental implementation of the exact configuration used in the simulation using the parameters given in Table 1.

4.1. Simulation results

While the actual distribution system can be more complicated, we modelled a radial system as in Fig. 6. The simulation diagram of the proposed D-STATCOM connected to an arbitrary n th bus is shown. A two-bus Thevenin equivalent (TE) is used to represent the

radial power system topology. At the bus of interest, the TE is assumed to model the power system behaviour accurately, as long as there are no system side changes [40]. The assumption of the constancy of system side parameters, represented by the Thevenin voltage source in series with impedance is justified in the absence of topology-changing events. In Ref. [41], the parameters of the Thevenin model are estimated based on sampling the discrete time sequence of voltage and current phasors at the bus of interest. The use of TE to model the system behaviour is a powerful tool which simplifies the analysis around the terminals of interest by replacing a power network with a voltage source in series with the driving point impedance at the location of interest.

The upstream portion of the network is represented as a balanced three-phase voltage source with series impedance Z_s , and the load side is represented by a constant PQ load in parallel with a three-phase rectifier to model the non-linear loads. The proposed D-STATCOM is shunt connected: the D-STATCOM consists of three-phase MC with a three-phase choke connected at the output side. FCS-MPC is used to control the operation of the D-STATCOM system.

4.1.1. Use case I: simulation results with three-phase non-linear load

The performance of the system with non-linear load has simulated and MATLAB/Simulink results are presented. Fig. 7 shows phase (A) source voltage and current before and after D-STATCOM is connected. As it can be seen from the figure, before the D-STATCOM is connected to the system the source current was highly distorted with THD of 26.88% as presented in the spectral analysis of phase (A) current in Fig. 8. When the D-STATCOM is enabled and connected to the PCC it can be seen that the source current becomes sinusoidal with THD of 2.99% as in Fig. 9.

The three-phase source voltages before and after D-STATCOM is connected is shown in Fig. 10. The THD of phase (A) voltage is shown in Fig. 11 and Fig. 12, and it can be seen that the voltage distortion has been reduced from 1.15% to 0.2% after the D-STATCOM is connected. Fig. 13 shows the simulation results of the D-STATCOM input current I_{cA} before and after D-STATCOM connection. When D-STATCOM is connected at $t = 0.1$, it can be seen that FCS-MPC was able to track the reference and the proposed D-STATCOM was able to inject the required harmonic components consumed by the load and keep the input source current sinusoidal.

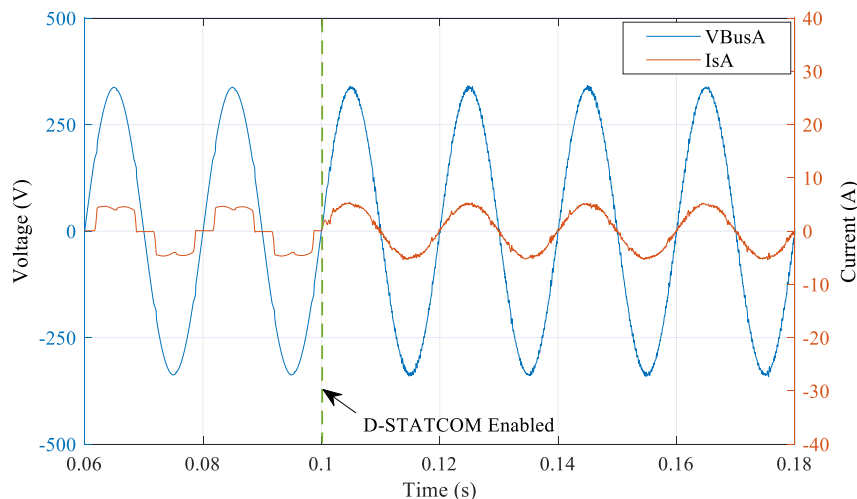


Fig. 7. Simulation results of the source voltage (V_{BusA}) and current (I_{sA}). Prior to enabling the D-STATCOM the source current is in-phase with the source voltage but contains considerable distortion. After the D-STATCOM is enabled the source current is in-phase with the source voltage and distortion free.

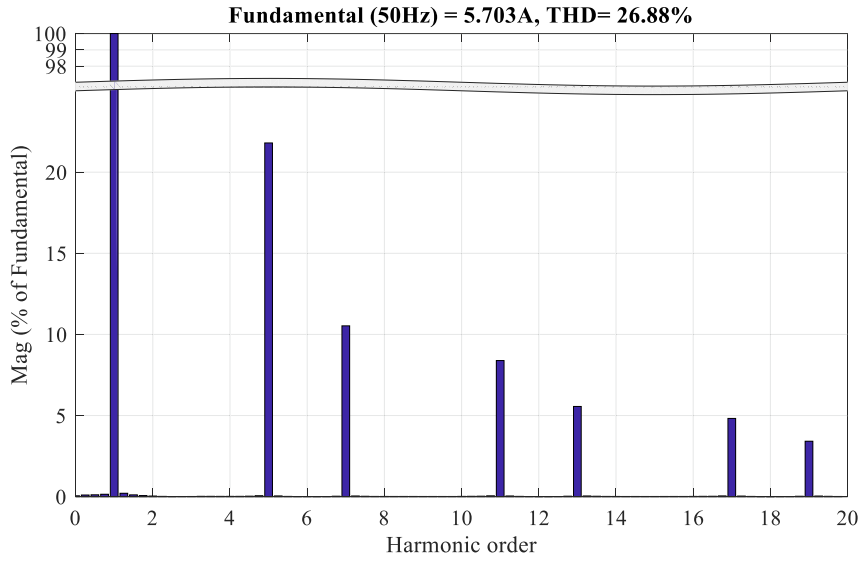


Fig. 8. Simulation results of source current spectral analysis (I_{sA}) before D-STATCOM is connected.

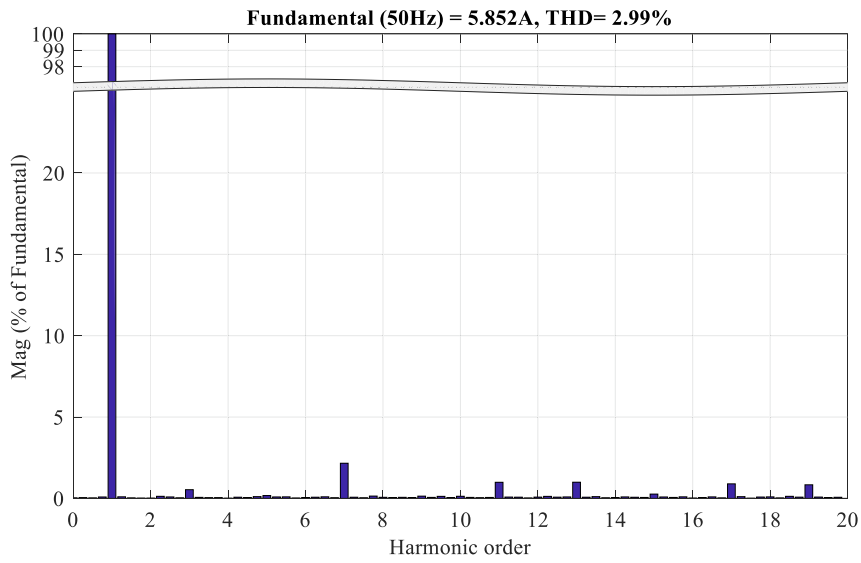


Fig. 9. Simulation results of source current spectral analysis (I_{sA}) after D-STATCOM is connected. THD reduced from 26.88% without compensation to 2.99% after enabling the D-STATCOM.

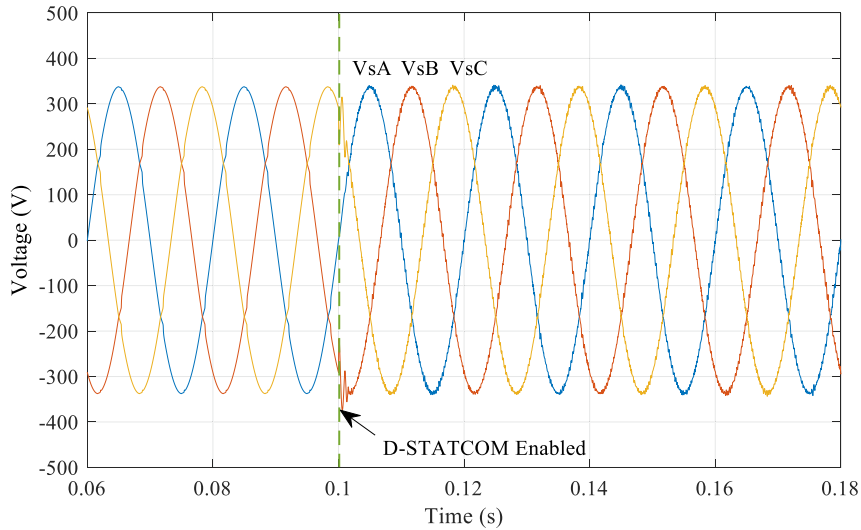


Fig. 10. Simulation results of the three-phase source voltage.

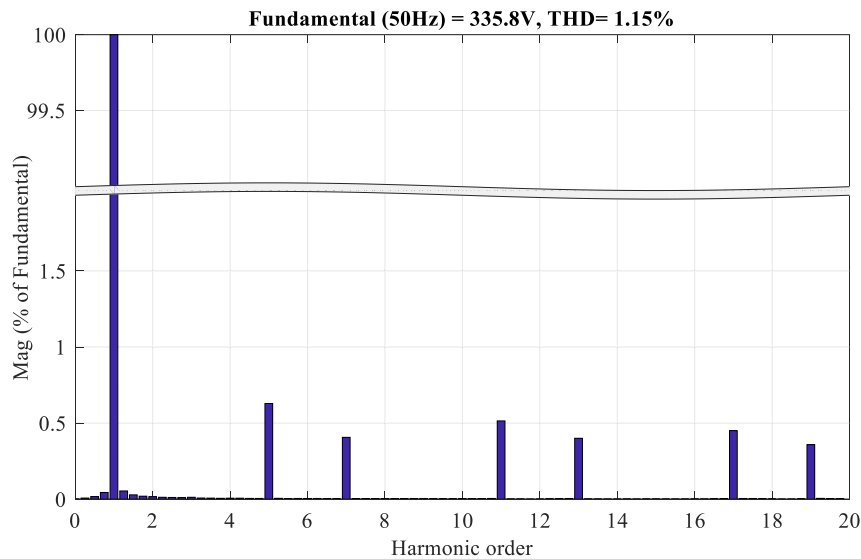


Fig. 11. Simulation results of source voltage spectral analysis (V_{BusA}) before D-STATCOM is connected.

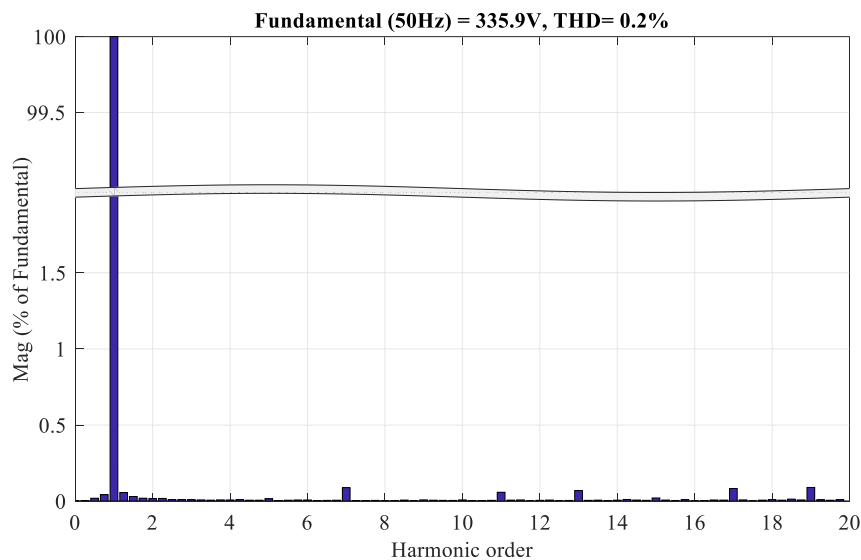


Fig. 12. Simulation results of source voltage spectral analysis (V_{BusA}) after D-STATCOM is connected.

4.1.2. Use case II: simulation results with three-phase non-linear and linear RL load

In order to demonstrate the effectiveness of proposed D-STATCOM in harmonics and power factor compensation, the performance was tested during non-linear and inductive loading. Fig. 14 shows the simulation results of source voltage and current before and after D-STATCOM is connected. It can be noticed that the D-STATCOM is connected at $t = 0.1$, and the D-STATCOM was able to provide the required compensation to make the source current sinusoidal. The THD of the source current before and after D-STATCOM is connected is shown in Fig. 15 and Fig. 16, and it can be seen that the THD is dropped significantly from 11.11% to 2.10%. Fig. 17 shows that there is good tracking between the reference and measured current of the D-STATCOM phase (A). Fig. 18 shows that active and reactive power flow in the system. It can be seen that before the D-STATCOM is connected all the reactive power required by the load is supplied by the source, and after D-STATCOM is

enabled at $t = 0.1$, the D-STATCOM starts to provide the required VAR and harmonic compensation.

4.2. Experimental results

An experimental test setup is used to test the proposed capacitor-less D-STATCOM and the MPC system. As shown in Fig. 19. The experimental setup includes an Upstream side (12KVA three-phase grid simulator NHR-9410), downstream side (variable three-phase inductive and non-linear load), D-STATCOM (7.5 KVA matrix converter unit with three phase inductors connected at its the output side), and control platform that is used to control the system is based on dSPACE Scalexio. The matrix converter unit consists of nine IGBT modules SK60GM123 rated at 1200V and 60 A. Each module consists of two parallel diodes with two antiparallel IGBT's connected in common emitter configuration, isolated gate drive circuit, current direction detection circuit, clamp circuit for

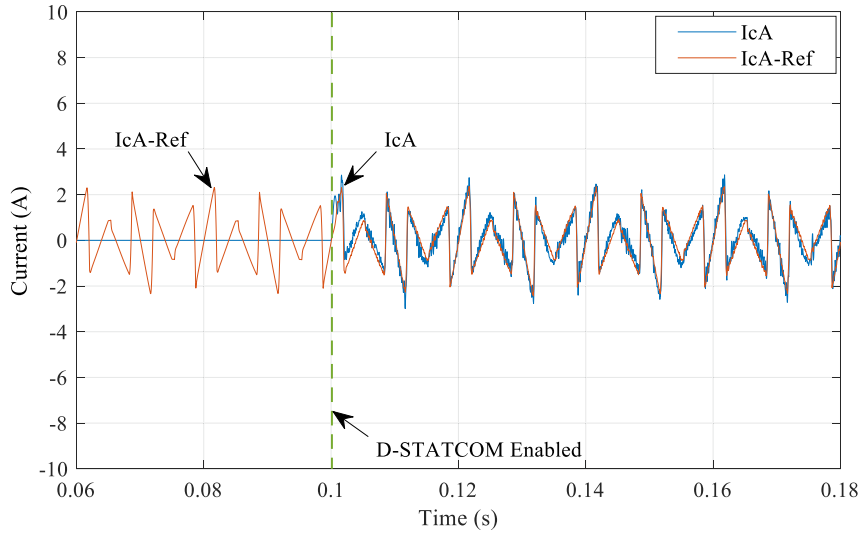


Fig. 13. Simulation results of reference current (I_{cA_Ref}) and the actual measured current (I_{cA}). After the D-STATCOM is enabled at $t=0.1$, good tracking between D-STATCOM measured and reference current is shown.

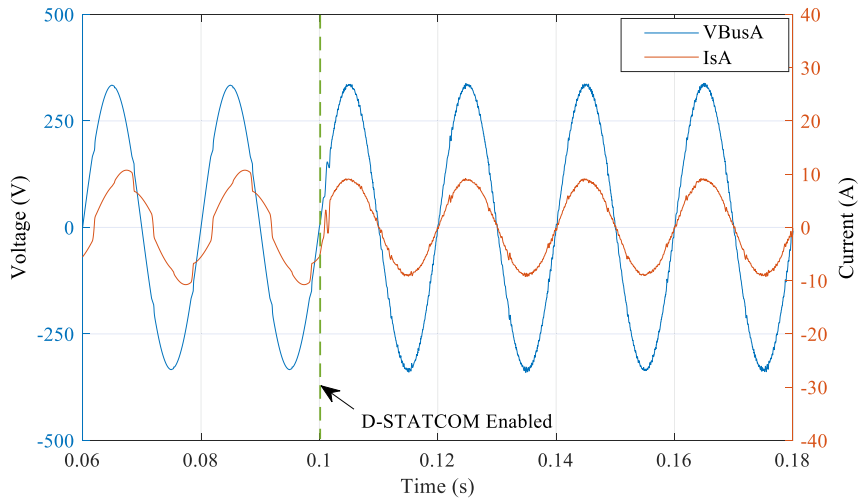


Fig. 14. Simulation results of the source voltage (V_{BusA}) and current (I_{sA}) with non-linear and linear loads. After the D-STATCOM is enabled the source current is in-phase with the source voltage and distortion free.

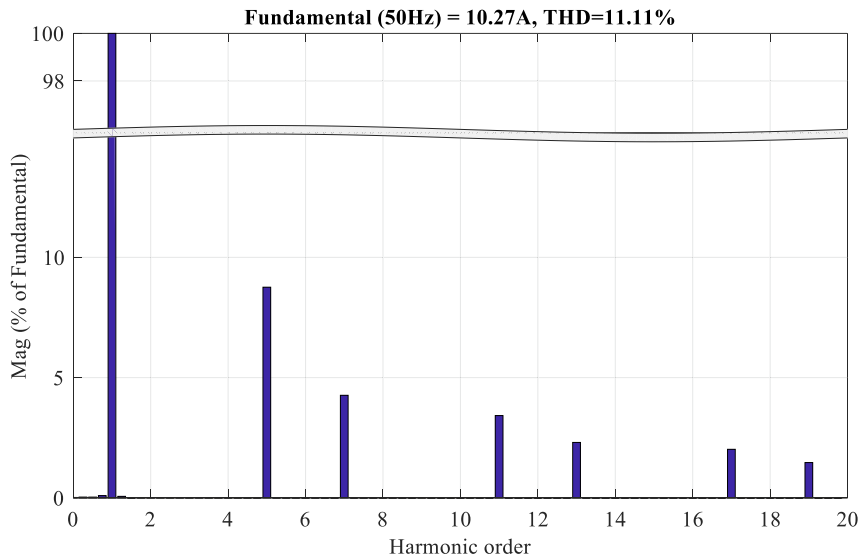


Fig. 15. Simulation results of source current spectral analysis (I_{sA}) before D-STATCOM is connected.

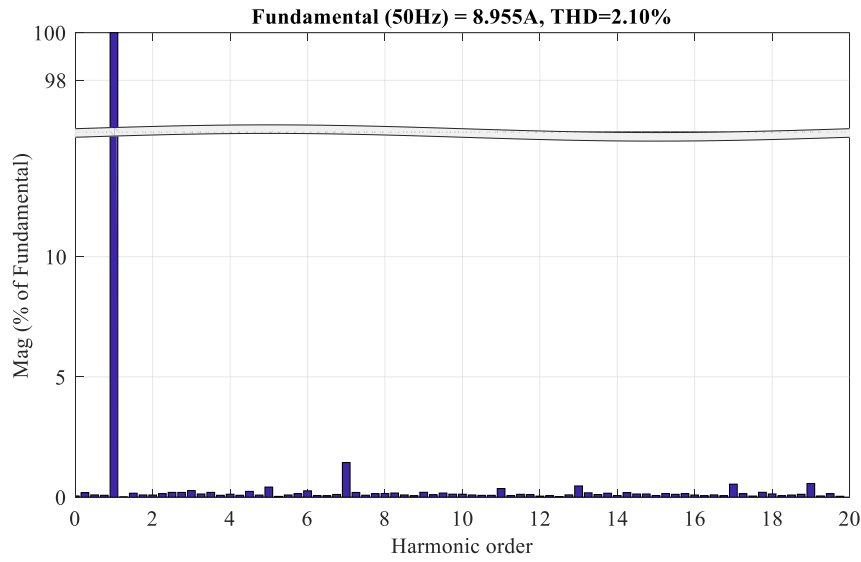


Fig. 16. Simulation results of spectral analysis of source current (I_{sA}) after D-STATCOM is connected.

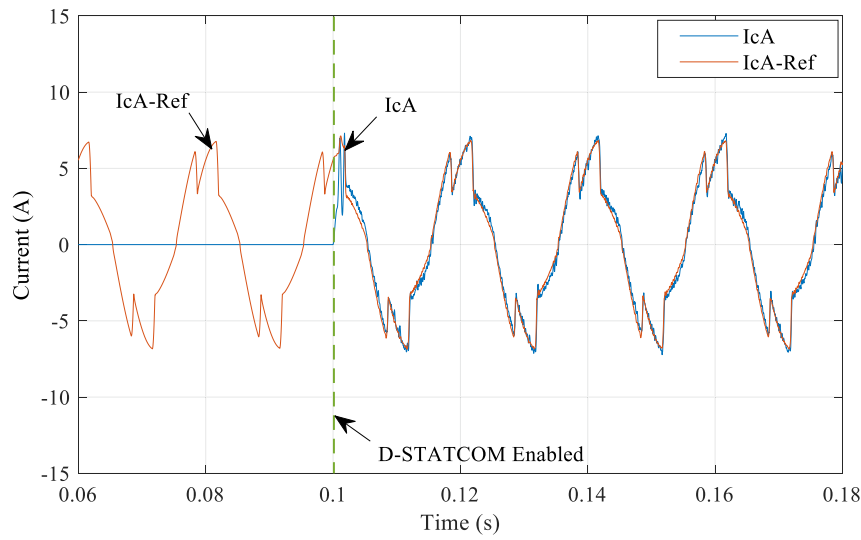


Fig. 17. Simulation results of source current (I_{cA}) during non-linear and inductive load condition. After the D-STATCOM is enabled at $t=0.1$, good tracking between D-STATCOM measured and reference current is shown.

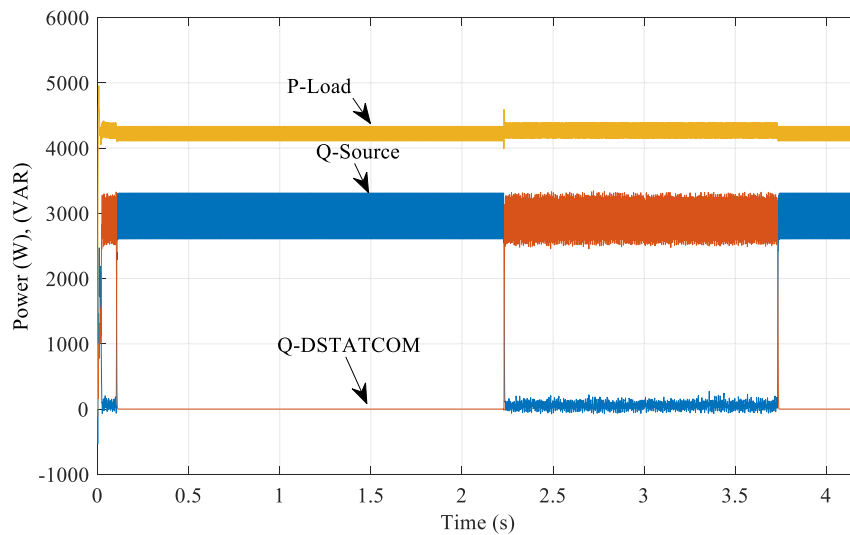


Fig. 18. Simulation results of source and D-STATCOM reactive power, and load active power.

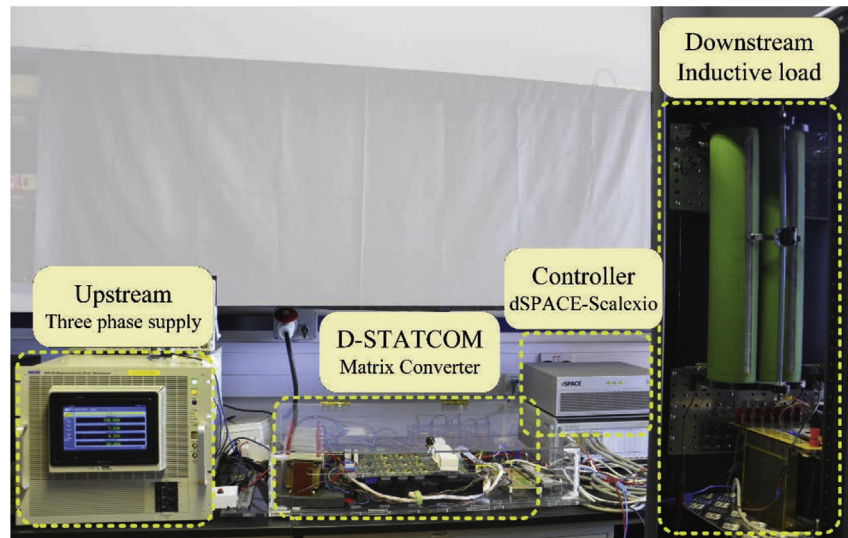


Fig. 19. Experimental setup of 7.5KVA D-STATCOM.

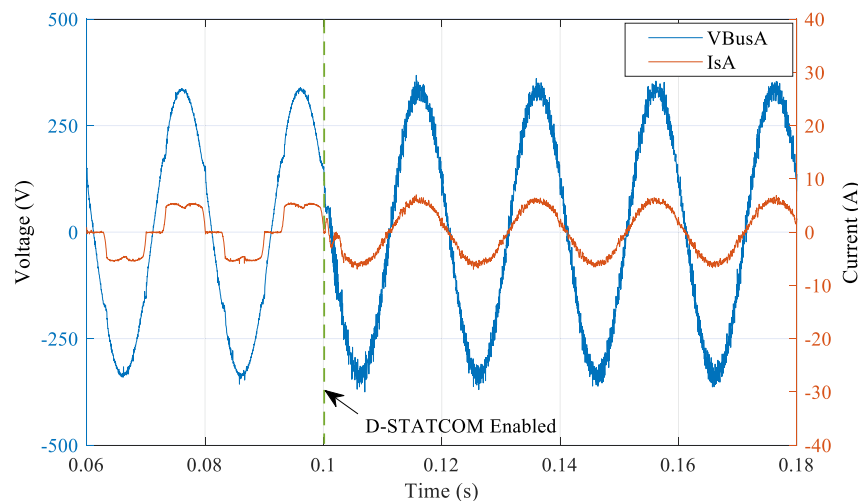


Fig. 20. Experimental results of upstream phase voltage (V_{BusA}) and current (I_{sA}). After the D-STATCOM is enabled the source current is in-phase with the source voltage and distortion free.

overvoltage protection, input voltage sensors LEM LV 25-p and output current sensors LEM LP 55. System parameters are summarized in Table 1. The dSPACE control platform consists of a processing unit and LabBox™ with 4 FPGA modules each module has 5 ADC 14bit resolution, 10 digital I/O pins and 5 analogue output pins. The MPC strategy is implemented in the dSPACE Scalexio processing unit, while the measurements and four step commutation and protection are implemented in dSPACE LabBox™ unit. dSPACE ControlDesk™ software is used to supervise and control the experiment in real-time and view and store the experimental results and modify the desired control parameters during the experiment.

Use case I: Experimental results with three-phase non-linear load

Initially, Fig. 20 present the experimental results of source voltages and currents waveforms supplying non-linear load before and after the connection of the D-STATCOM. D-STATCOM is

connected at $t = 0.1$, and it can be seen that the source current is distorted before the connection the D-STATCOM and the THD is 26.99% as presented in Fig. 21. When the D-STATCOM is connected at $t = 0.1$, it is clear that the D-STATCOM was able to compensate for the load current harmonics and inject the required current to keep the source current sinusoidal. Fig. 22 shows the spectral analysis of the source current and it can be seen that the THD was drastically reduced from 26.99% before compensation to 3.43% after compensation. Fig. 23 present the three-phase source voltage. And it is clear that the source voltage THD was reduced after the connection of the D-STATCOM from 2.65% to 0.63% as illustrated in Fig. 24 and Fig. 25. Fig. 26 present how the D-STATCOM input current tracks the reference with good accuracy.

4.2.1. Use case II: experimental results with three-phase non-linear and linear RL load

In this use case, the performance of the proposed D-STATCOM was tested during non-linear and inductive loading. Fig. 27 shows the experimental results of source voltage and current

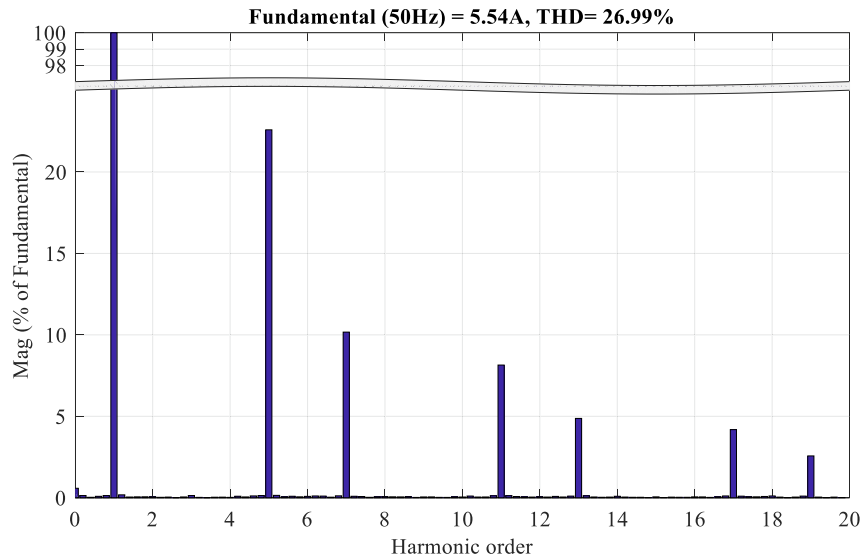


Fig. 21. Experimental results of source current spectral analysis (I_{sA}) before D-STATCOM is connected.

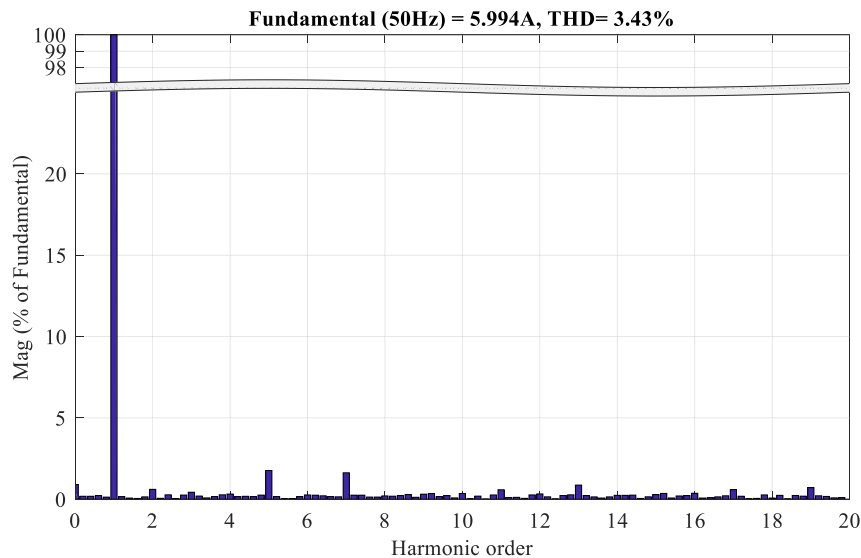


Fig. 22. Experimental results of source current spectral analysis (I_{sA}) after D-STATCOM is connected.

before and after D-STATCOM is connected. It can be noticed that the D-STATCOM is connected at $t = 0.1$, and the D-STATCOM was able to provide the required compensation to make the source current sinusoidal. The THD of the source current before and after D-STATCOM is connected is shown in Fig. 28 and Fig. 29, and it can be observed that the THD was dropped significantly from 13.62% to 3.65%. Fig. 30 shows that there is good tracking between the reference and measured current of the D-STATCOM phase (A). Fig. 31 shows the experimental results of the active and reactive power flow in the system. It can be seen that before the D-STATCOM is connected all the reactive power required by the load is supplied by the source, and after D-STATCOM is enabled the source reactive power dropped to zero and the D-STATCOM starts to provide the required VAR and harmonic compensation.

5. Conclusion

This paper proposed a capacitor-less D-STATCOM based on MC and controlled using FCS-MPC for harmonic current mitigation and power factor correction, which results due to the use of non-linear loads in the modern electrical distribution network. The instantaneous control of the active and reactive power is accomplished by the SRF method and FCS-MPC. In this manner, the shunt-connected, D-STATCOM, mitigates the harmonic pollution at the source, thus preventing the propagation of undesirable harmonics, which can disrupt the smooth operation of other devices and can lead to overheating issues in lines and substation transformer windings.

The main advantages of the proposed solution is the use of inductive storage rather than capacitive elements ensures the longevity of such a power quality compensator and makes it well

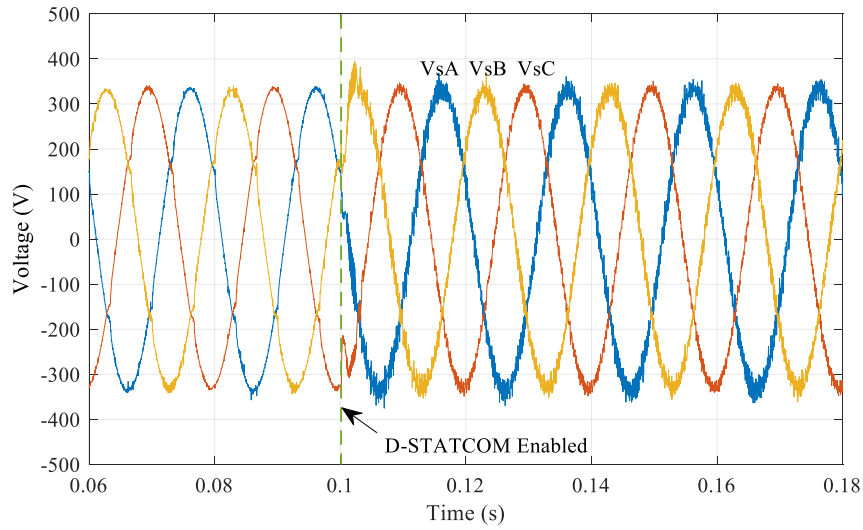


Fig. 23. Experimental results of upstream voltage before and after D-STATCOM is connected.

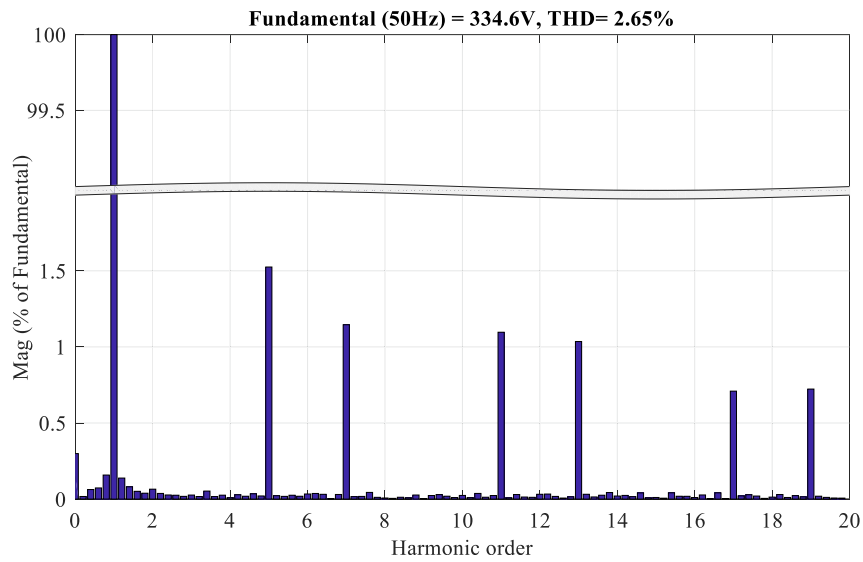


Fig. 24. Experimental results of source voltage spectral analysis (V_{BUSA}) before D-STATCOM is connected.

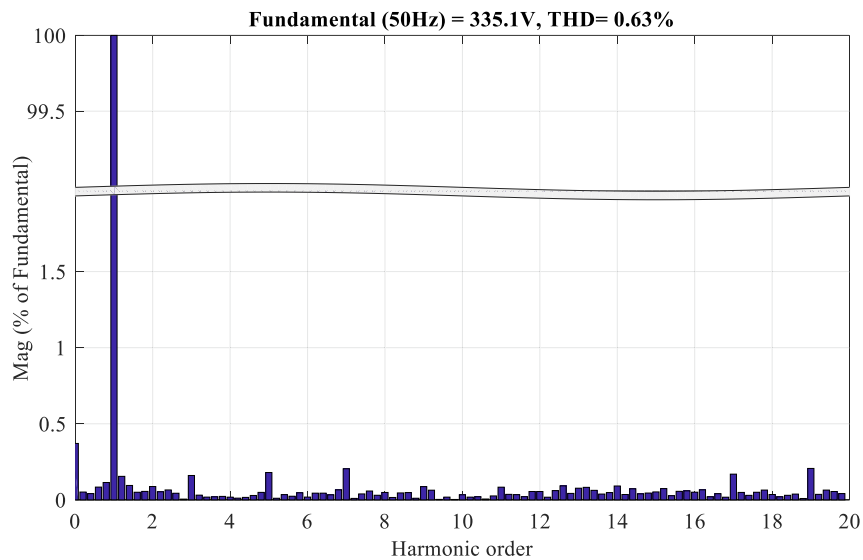


Fig. 25. Experimental results of source voltage spectral analysis (V_{BUSA}) after D-STATCOM is connected.

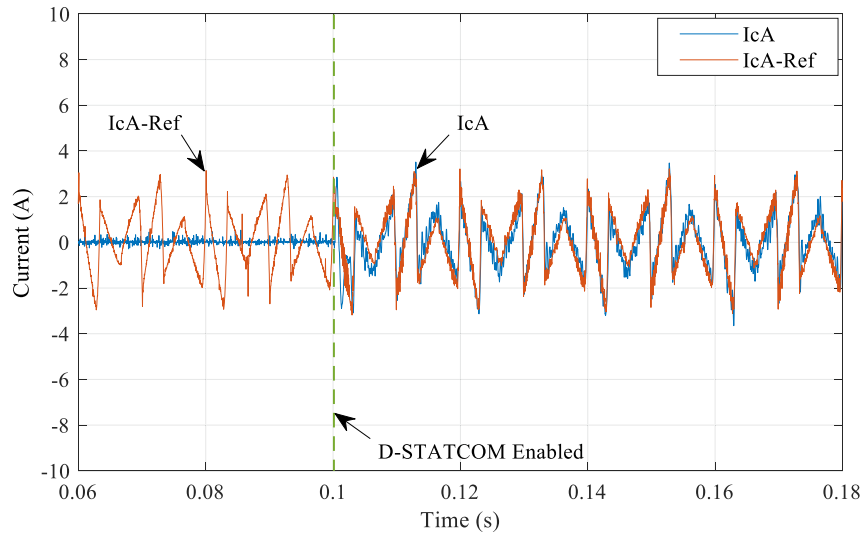


Fig. 26. Experimental results of D-STATCOM input current (I_{cA}) tracking the reference current (I_{cA-Ref}). After the D-STATCOM is enabled at $t=0.1$, good tracking between D-STATCOM measured and reference current is shown.

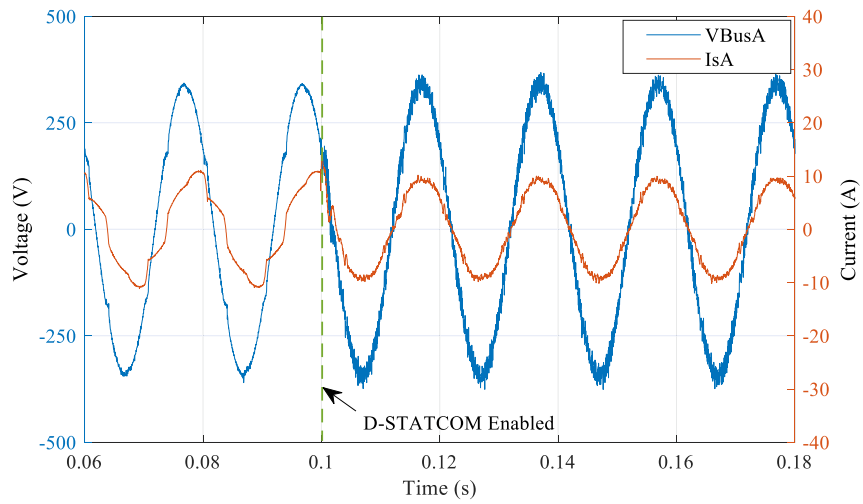


Fig. 27. Experimental results of upstream phase voltage (V_{BusA}) and current (I_{sA}). After the D-STATCOM is enabled the source current is in-phase with the source voltage and distortion free.

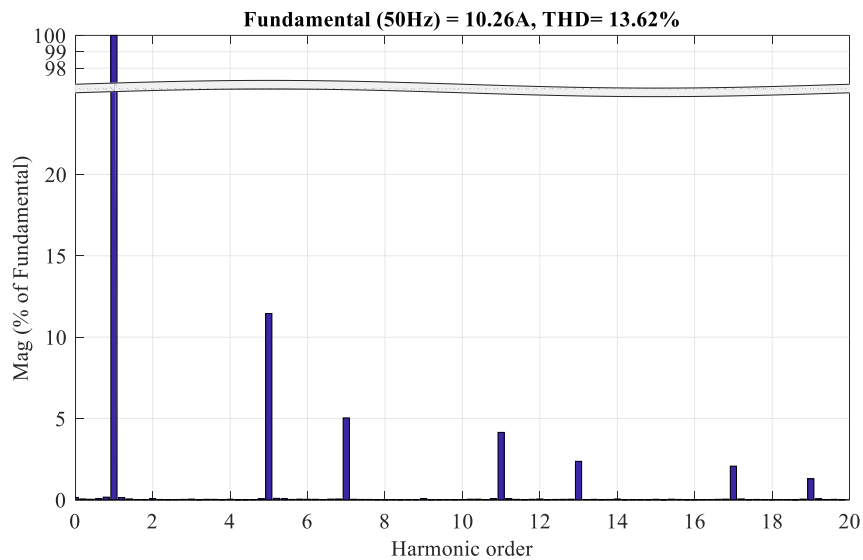


Fig. 28. Experimental results of source current spectral analysis (I_{sA}) before D-STATCOM is connected.

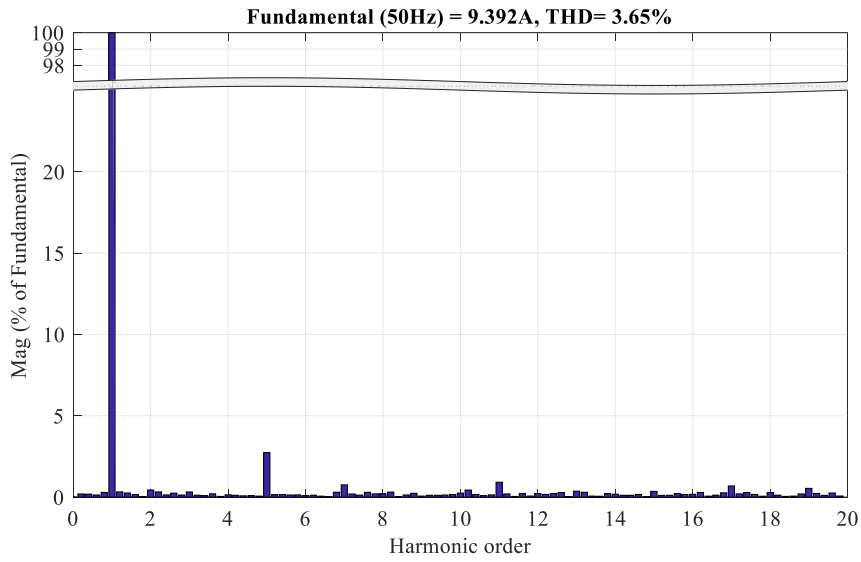


Fig. 29. Experimental results of source current spectral analysis (I_{cA}) after D-STATCOM is connected.

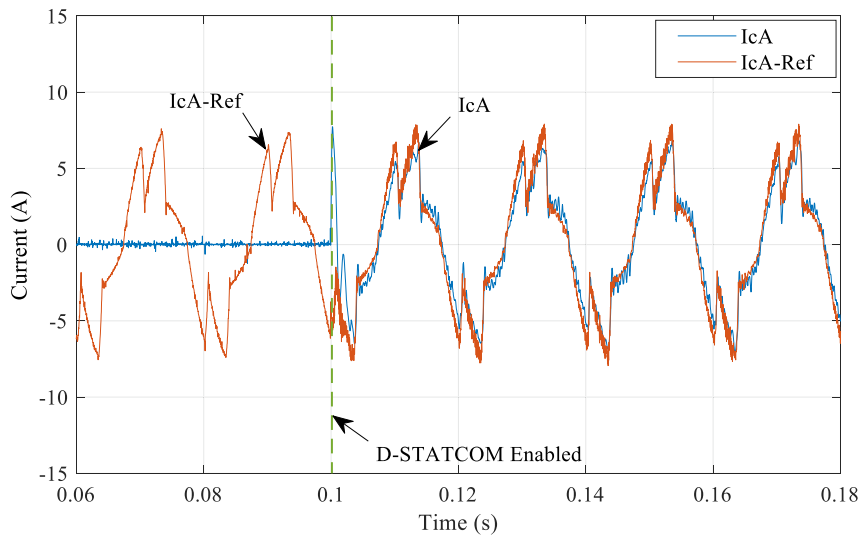


Fig. 30. Experimental results of D-STATCOM input current (I_{cA}) tracking the reference current (I_{cA-Ref}) use case II. After the D-STATCOM is enabled at $t=0.1$, good tracking between D-STATCOM measured and reference current is shown.

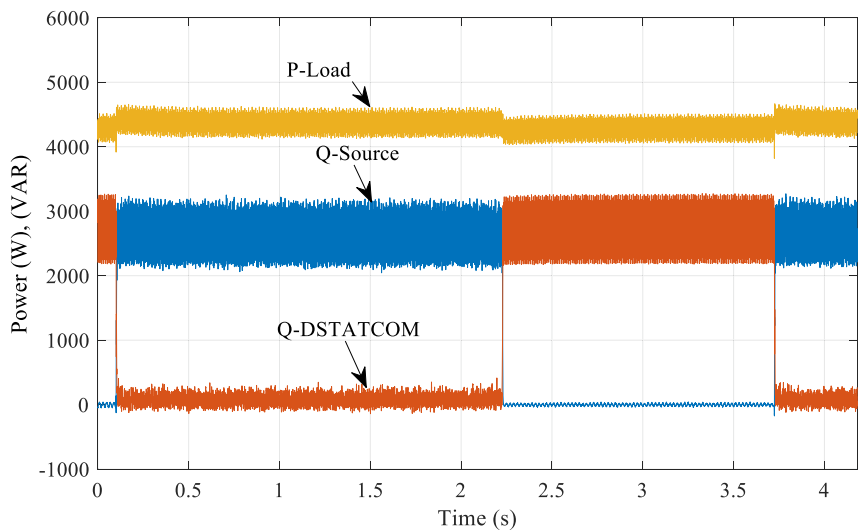


Fig. 31. Experimental results are showing load active power (P-Load), source reactive power (Q-Source) and D-STATCOM reactive power (Q-DSTATCOM).

sued for counties known for hot and arid climate conditions. Furthermore, the use of MPC makes the control of the D-STATCOM is robust and flexible to add control variables in the cost function to provide more attractive features in the future such as voltage profile control, and switching losses reduction.

Simulation and experimental results of the different use cases presented in this paper show that the proposed capacitor-less D-STATCOM is able to provide the required power factor correction and harmonic mitigation to the non-linear loads connected at the low voltage side of the distribution network. In the future, the performance of the D-STATCOM will be studied to provide voltage regulation.

Acknowledgement

This publication was made possible by NPRP grant # 9-204-2-103 from the Qatar National Research Fund (a member of Qatar Foundation). The statements made herein are solely the responsibility of the authors.

References

- [1] N.A. Armstrong, The Engineered Century: a century hence, 2000 may be viewed as quite a primitive period in human history. It's something to hope for, *Bridge* 30 (1) (2000) 14–18. Spring.
- [2] H.L. Willis, R.R. Schrieber, *Aging Power Delivery Infrastructures*, CRC Press, 2016.
- [3] M.J. Sullivan, M. Mercurio, J. Schellenberg, Estimated Value of Service Reliability for Electric Utility Customers in the United States, Ernest Orlando Lawrence Berkeley National Laboratory, Berkeley, CA, 2009.
- [4] M. Shuai, W. Chengzhi, Y. Shiwen, G. Hao, Y. Jufang, H. Hui, Review on economic loss assessment of power outages, *Procedia Comput. Sci.* 130 (2018) 1158–1163, 2018/01/01.
- [5] H. De Keulenaer, The Hidden Cost of Poor Power Quality, European copper institute, 2003.
- [6] N. Adam, Workshop on future directions in cyber-physical systems security, in: Report on Workshop Organized by Department of Homeland Security (DHS), 2010.
- [7] The Value of Electricity when It's Not Available, The National Renewable Energy Laboratory, 2003. NREL/BR-200-34231.
- [8] I. Utu, D. Pasculescu, Power quality study in order to comply with European Norms, *Calitatea* 18 (S1) (2017) 366.
- [9] D. Chapman, The cost of poor power quality, in: *Power Quality Application Guide*, Copper Development Association, 2001.
- [10] W. Rohouma, R.S. Balog, A.A. Peerzada, M.M. Begovic, D-STATCOM for a distribution network with distributed PV generation, in: Presented at the International Conference on Photovoltaic Science and Technologies (PVCon), 2018, 4–6 July.
- [11] J.A. Martinez, J. Martin-Arnedo, Impact of distributed generation on distribution protection and power quality, in: Presented at the IEEE Power & Energy Society General Meeting, 2009, pp. 26–30. July.
- [12] S. Sahoo, Impact Study: Photo-Voltaic Distributed Generation on Power System, 2016.
- [13] C.-S. Lam, M.-C. Wong, *Design and Control of Hybrid Active Power Filters*, Springer, 2014.
- [14] C. Po-Tai, S. Bhattacharya, D. Divan, Experimental verification of dominant harmonic active filter for high-power applications, *IEEE Trans. Ind. Appl.* 36 (2) (2000) 567–577.
- [15] R. Torquato, F.C.L. Trindade, W. Freitas, Analysis of the harmonic distortion impact of photovoltaic generation in Brazilian residential networks, in: Presented at the 16th International Conference on Harmonics and Quality of Power (ICHQP), 2014, 25–28 May.
- [16] S. Bhattacharyya, J.M.A. Myrzik, W.L. Kling, Consequences of poor power quality - an overview, in: 2007 42nd International Universities Power Engineering Conference, 2007, pp. 651–656.
- [17] P. Acuna, L. Moran, M. Rivera, J. Dixon, J. Rodriguez, Improved active power filter performance for renewable power generation systems, *IEEE Trans. Power Electron.* 29 (2) (2014) 687–694. Feb.
- [18] U. Das Gupta, P. Das, M.A. Hoque, A fuzzy controlled shunt active power filter for reducing current harmonics and reactive power compensation, in: Presented at the 2015 International Conference on Electrical Engineering and Information Communication Technology (ICEEICT), 2015, 21–23 May.
- [19] L. Qian, P. Li, K. Yong, T. Shiyang, W. Deliang, Q. Yu, A novel design and optimization method of an LCL filter for a shunt active power filter, *IEEE Trans. Ind. Electron.* 61 (8) (2014) 4000–4010. Aug.
- [20] M. El-Habrouk, M.K. Darwish, P. Mehta, Active power filters: a review, *IEE Proc. Electr. Power Appl.* 147 (5) (2000) 403–413.
- [21] R.N. Beres, X. Wang, M. Liserre, F. Blaabjerg, C.L. Bak, A review of passive power filters for three-phase grid-connected voltage-source converters, *IEEE J. Emerg. Select. Top. Power Electron.* 4 (1) (2016) 54–69.
- [22] R.S. Rani, C.S. Rao, M.V. Kumar, Analysis of active power filter for harmonic mitigation in distribution system, in: Presented at the 2016 International Conference on Electrical, Electronics, and Optimization Techniques (ICEEOT), 2016, 3–5 March.
- [23] D. Schwanz, M. Bollen, A. Larsson, Ł.H. Kocewiak, Harmonic mitigation in wind power plants: active filter solutions, in: Presented at the 2016 17th International Conference on Harmonics and Quality of Power (ICHQP), 2016, 16–19 Oct.
- [24] T. Demirdelen, M. Inci, K.C. Bayindir, M. Tumay, Review of hybrid active power filter topologies and controllers, in: Presented at the Fourth International Conference on Power Engineering, Energy and Electrical Drives (POWERENG), 2013, 13–17 May.
- [25] B. Singh, K. Al-Haddad, A. Chandra, A new control approach to three-phase active filter for harmonics and reactive power compensation, *IEEE Trans. Power Syst.* 13 (1) (1998) 133–138.
- [26] B. Singh, A. Chandra, K. Al-Haddad, *Power Quality: Problems and Mitigation Techniques*, John Wiley & Sons, 2014.
- [27] S. Harb, R.S. Balog, Reliability of candidate photovoltaic module-integrated-inverter (PV-MII) topologies-A usage model approach, *IEEE Trans. Power Electron.* 28 (6) (2013) 3019–3027.
- [28] C. Lachkar, et al., Failure analysis of aluminum electrolytic capacitors based on electrical and physicochemical characterizations, in: Presented at the 2017 IEEE International Reliability Physics Symposium (IRPS), 2017, 2–6 April.
- [29] T. Orłowska-Kowalska, F. Blaabjerg, J. Rodríguez, *Advanced and Intelligent Control in Power Electronics and Drives*, Springer, 2014.
- [30] S. Yang, A. Bryant, P. Mawby, D. Xiang, L. Ran, P. Tavner, An industry-based survey of reliability in power electronic converters, *IEEE Trans. Ind. Appl.* 47 (3) (2011) 1441–1451.
- [31] L.F. Costa, M. Liserre, Failure analysis of the dc-dc converter: a comprehensive survey of faults and solutions for improving reliability, *IEEE Power Electron. Mag.* 5 (4) (2018) 42–51.
- [32] H. Akagi, E.H. Watanabe, M. Aredes, *Instantaneous Power Theory and Applications to Power Conditioning*, John Wiley & Sons, 2017.
- [33] F. Blaabjerg, *Control of Power Electronic Converters and Systems*, Academic Press, 2018.
- [34] S. Bhattacharya, D. Divan, Synchronous frame based controller implementation for a hybrid series active filter system, in: Presented at the Industry Applications Conference, Thirtieth IAS Annual Meeting, 1995, 8–12 Oct.
- [35] B. Singh, V. Verma, Selective compensation of power-quality problems through active power filter by current decomposition, *IEEE Trans. Power Deliv.* 23 (2) (2008) 792–799.
- [36] M.B. Shadmand, M. Mosa, R.S. Balog, H. Abu-Rub, Model predictive control of a capacitorless matrix converter-based STATCOM, *IEEE J. Emerg. Select. Top. Power Electron.* 5 (2) (2017) 796–808.
- [37] W. Rohouma, R.S. Balog, A.A. Peerzada, M.M. Begovic, Capacitor-less D-STATCOM for reactive power compensation, in: Presented at the IEEE 12th International Conference on Compatibility, Power Electronics and Power Engineering (CPE-POWERENG), 2018, 10–12 April.
- [38] M.B. Shadmand, R.S. Balog, H. Abu-Rub, Auto-tuning the cost function weight factors in a model predictive controller for a matrix converter VAR compensator, in: Presented at the IEEE Energy Conversion Congress and Exposition (ECCE), Montreal, Canada, 2015. Sept.
- [39] P. Cortes, et al., Guidelines for weighting factors design in Model Predictive Control of power converters and drives, in: Presented at the IEEE International Conference on Industrial Technology, 2009. Feb.
- [40] M. Begovic, A. Peerzada, R. Nuqui, B. Picone, On networked VIP monitoring of voltage stability, in: Presented at the Proceedings, 2017.
- [41] M. Begovic, A. Peerzada, R. Nuqui, B. Picone, Locational Accuracy of VIP Indices for Voltage Collapse Margin Estimation, 2018.